Theoretical and Experimental Analysis of the Destabilization of Modes Driven by Fast Particles in Tore-Supra

C. Nguyen[1], A. Merle[2], Z.O. Guimaraes-Filho[3], X. Garbet[2], R. Sabot[2], J. Decker[2], L.-G. Eriksson[4], M. Goniche[2], G. Huysmans[2], H. Lütjens[1], P. Maget[2].
[1]CPhT, CNRS-Ecole Polytechnique, France.
[2]CEA, IRFM, F-13108 Saint-Paul-lez-Durance, France.
[3]PIIM, CNRS-Université de Provence, France.
[4]European Commission, Research Directorate General, B-Brussels, Belgium.
christine.nguyen@cpht.polytechnique.fr

Abstract A necessary step towards the control of burning plasmas is the understanding of instabilities driven by suprathermal particles, which are known to be dangerous for the plasma confinement. The mechanisms underlying their destabilization are studied for two modes identified in Tore-Supra. Linearly, experimental and analytical evidences are presented which show the strong sensitivity of the fast electron driven fishbone stability on the current profile, and the non-negligible role of diamagnetic effects and fast particle induced non-perturbative effects on non-chirping steady-state Beta Alfvén Eigenmodes. Nonlinearly, the main damping mechanism acting on Beta Alfvén Eigenmodes is shown to enable the existence of subcritical modes.

1 Introduction

On the way towards the understanding of burning plasmas, studies of heating induced suprathermal populations are of major importance. Such populations are known to excite Magneto-HydroDynamic (MHD) modes which can have deleterious effects on the plasma energy confinement. In Tore-Supra, Ion Cyclotron Resonance Heating (ICRH) induced suprathermal ions are found to drive acoustic modes called Beta Alfvén Eigenmodes (BAEs) [1, 2]. Lower Hybrid (LH) heated electrons are also thought to excite meso-scale modes called fishbone modes albeit characterized by smaller radio-gyradii, which is a good indicator that energy is the main parameter of the plasma-fast particle interaction, and that the dynamics studied in current devices is relevant to what should occur in larger reactor-size devices.

In the present work, we report on various experimental and theoretical studies carried out in Tore-Supra, to understand the mechanisms and conditions underlying the interaction of suprathermal particles with MHD modes. An upgrade of the reflectometry and Electron Cyclotron Emission diagnostics associated with correlation and fitting techniques makes possible to access the modes radial structure, which reveals noteworthy dynamics at the current diffusion time scale. Such observations motivate a detailed analysis of the two modes linear stability, and in particular of the role of diamagnetic effects, non-perturbative fast particle induced kinetic effects and current profile shaping. Such accurate analysis is necessary to enable a control of fast particle driven modes, as well as for MHD based plasma diagnostics. In section 2, Tore-Supra experimental observations and parameters are outlined. Next, the model and results of the linear analysis of the modes stability are given in section 3. Finally, on a more theoretical side, the role of nonlinear effects such as particle wave-trapping in the stability of the Beta-Alfvén Eigenmodes are investigated in section 4.

2 Experimental parameters and radial structure of fast particle driven modes

Tore-Supra fast particle induced modes have been detected on the reflectometry and Electron Cyclotron Emission (ECE) diagnostics. Reflectometry is made of 2 channels, and ECE of 32 channels

which can be adjusted in one line of sight of the equatorial plane, hence allowing for a reconstruction of the modes radial structure and providing information on the mode poloidal mode number parity. For both BAEs and fishbones, a particular cyclical dynamics of the oscillation structures is found, which appears in close relation with the evolution of their frequency, as presented in Figs. 1, 2.

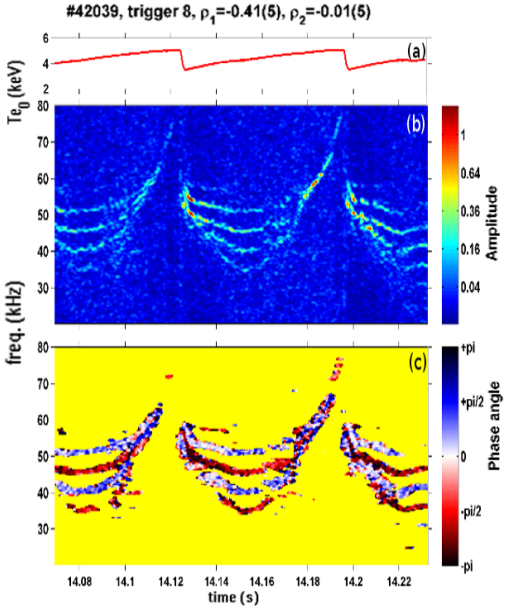

Figure 1: BAE cycle during a sawtooth period. a) is the core electron temperature, b) the reflectometry frequency spectrum and c) the phase angle between low and high field side perturbations for shot #42039. d) is the BAE radial structure obtained with ECE for an equivalent shot #44831.

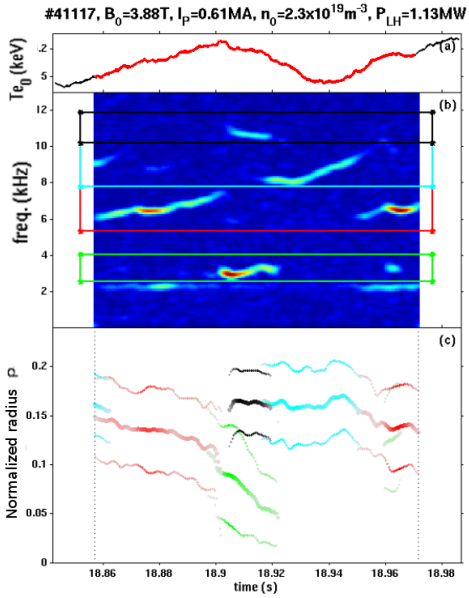

Figure 2: Fishbone cycle. a) is the core electron temperature b) the ECE frequency spectrum c) the mode radial structures obtained from a fit of the ECE signals.

2.1 Beta Alfvén Eigenmodes

BAEs have been found in sawtoothing high density discharges ($\sim 4 \times 10^19\mathrm{m}^{-3}$) characterized by a core electron temperature of about 4-5 keV, and a plasma current of 0.9-0.95 MA, in the presence of ICRH of typical power 2MW to 4.6 MW [2]. For the shot #42039, shown in Fig. 1 and analyzed below, the simulation of the current profile by the CRONOS transport code [3], returns a monotonic q-profile with q=1 surface at a normalized radius of 0.32. At this point, the density is equal to $n = 3.7 \times 10^{19}\mathrm{m}^{-3}$, the core ion temperature (obtained from the TPROF fit of neutron emission data [3]) to $T_i = 2.1$ keV, the ratio of core electron to core ion temperatures to 1.3, the typical density and temperature scales are $\nabla n/n = -1.5\mathrm{m}^{-1}$ and $\nabla T_i/T_i = -3.1\mathrm{m}^{-1}$.

As shown in Fig.1b. and c., several modes are found to oscillate in the acoustic frequency range (around 50 kHz). Radially, the analysis of the three most intense modes shows that they are all localized inside the $q = 1$ surface, almost stable during the sawtooth period, yet with a slight radial slight [4]. Poloidally, phase-angle analysis of low-field and high-field side perturbations (Fig. 1c.) suggests that the multiplicity of modes corresponds to modes with different poloidal mode numbers. Now looking at their frequency spectrum (Fig.1b.), a particular dynamics comes forth. While quasi steady state at the millisecond time scale, the mode frequencies display a downwards-upwards cycle which matches the sawtooth period, and is more pronounced for the lower branches, leading to a splitting and merging of the modes. This dynamics is reminiscent of observations performed at Asdex-Upgrade [5], and suggests a role of temperature and mode number related physics, such as diamagnetic effects.

2.2 Electron fishbone modes

Lower frequency modes with frequencies ranging from 8 to 14 kHz have been detected in discharges with typical density of 2-3$e19\mathrm{m}^{-3}$, a central temperature of about 4 keV, a plasma current of 0.6MA and in the presence of 1 to 2MW of LH heating. They have been identified as fishbone modes, in their quasi steady-state (non-bursting) regime also identified in Ref.[6]. As was reported in Ref.[7], the frequency of these modes is characterized by jumps illustrated in Fig. 2b., associated to modulations of the central temperature, sometimes in the form of a neat oscillation (Fig. 2a.) with a time scale corresponding to a current diffusion time scale.

Using the matching techniques described in Ref.[8], the radial localization of the modes has been determined (Fig 2c.). It shows that the frequency jumps are associated to a continuous inward drift of a mode, and the apparition of a second mode at the first mode initial position, close to a $q = 1$ surface provided by the CRONOS transport code at the normalized radius 0.16. Remarkably, the discontinuous frequency jumps are associated to continuous evolutions of the mode position.

This evolution of the mode structure suggests a modication of equilibrium properties. More precisely, the correlation between the mode localization and a q=1 surface and the slow inward drift of one of the modes advocates for a cycle of the central q-profile, not accessible to a sufficient accuracy by the simulation. Moreover, the discontinous transition between modes indicates that this q-profile oscillation has a strong impact on stability. Such observations suggests the necessity of a detailed analysis of the role of the q-profile in the electron fishbone stability.

3 Linear analysis of the mode stability and oscillation frequency

3.1 Developed tools

As was shown in Ref. [9], the linear dispersion relation of fast particle driven modes of the low shear Alfvén spectrum can be put in the same form

$$i\Lambda|s| = \delta\hat{W}_f + \delta\hat{W}_k \tag{1}$$

where Λ represents the thermal plasma inertia including second order Finite Larmor Radius effects, $\delta\hat{W}_f$ is the normalized plasma non-resonant fluid energy and $\delta\hat{W}_k$ is the normalized kinetic resonant contribution of fast particles.

Multiple derivations of Λ for BAEs [10, 11, 12, 13, 14] and for fishbone modes [15, 16, 17] exist, which can be consistently combined [10]. In this work, we considered Λ to be the square root of Λ^2 such that $\partial\Lambda_r/\partial\omega_r > 0$, where,

$$\Lambda^2 = 3\frac{\omega(\omega-\omega_{*i})}{\omega_A^2} \quad \text{for the lower frequency spectrum (Fishbone)} \tag{2}$$

$$\Lambda^2 = \frac{\omega^2}{\omega_A^2}\left(1-\frac{\omega^{\mathrm{m}}_{*pi}}{\omega}\right)+q^2\frac{\omega\omega_{ti}}{\omega_A}\left[\left(1-\frac{\omega^{\mathrm{m}}_{*ni}}{\omega}\right)F\left(\frac{\omega}{\omega_{ti}}\right)-\frac{\omega^{\mathrm{m}}_{*Ti}}{\omega}G\left(\frac{\omega}{\omega_{ti}}\right)\right.$$
$$\left.-\frac{N^{\mathrm{m}}(\omega/\omega_{ti})}{2}\left\{\frac{N^{\mathrm{m}+1}(\omega/\omega_{ti})}{D^{\mathrm{m}+1}(\omega/\omega_{ti})}+\frac{N^{\mathrm{m}-1}(\omega/\omega_{ti})}{D^{\mathrm{m}-1}(\omega/\omega_{ti})}\right\}\right] \quad \text{for the higher spectrum (BAE)} \tag{3}$$

In these formulas, corresponding to the derivation of Ref. [10] with the poloidal non-degeneracy correction added in Ref. [12], $F(x) = x(x^2+3/2)+(x^4+x^2+1/2)Z(x)$, $G(x) = x(x^4+x^2+2)+(x^6+x^4/2+x^2+3/4)Z(x)$, $N^{\mathrm{m}}(x) = (1-\omega^{\mathrm{m}}_{*ni}/\omega)[x+(1/2+x^2)Z(x)]-(\omega^{\mathrm{m}}_{*Ti}/\omega)[x(1/2+x^2)+(1/4+x^4)Z(x)]$, $D^{\mathrm{m}}(x) = (1/x)(1+1/\tau_e)+(1-\omega^{\mathrm{m}}_{*ni}/\omega)Z(x)-(\omega^{\mathrm{m}}_{*Ti}/\omega)[x+(x^2-1/2)Z(x)]$. (m,n) represent the main poloidal and toroidal mode numbers, $\omega_A = v_A/qR$ with v_A the Alfvén velocity, R the major radius and q the safety factor at the mode resonance surface r_s, $\omega_{ti} = v_{ti}/qR$ with $v_{ti} =$

$\sqrt{2T_i/m_i}$ the core ion thermal velocity, and $\tau_e = T_e/T_i$ with T_i and T_e the equilibrium core electron and core ion temperatures. Diamagnetic effects are taken into account via the quantities $\omega^{\mathsf{m}}_{*Ti} = (\mathsf{m}/r)(T_i/e_iB_0)(\nabla_r T_i/T_i)$, $\omega^{\mathsf{m}}_{*ni} = (\mathsf{m}/r)(T_i/e_iB_0)(\nabla_r n_i/n_i)$, $\omega^{\mathsf{m}}_{*pi} = \omega_{*Ti} + \omega_{*ni}$.

$\delta\hat{W}_f$ depends on the mode global structure. For an $|n| = |m| = 1$ kink structure, expected for a traditional fishbone mode and possible for an $|\mathsf{n}| = |\mathsf{m}| = 1$ BAE [17, 13], it is [18]:

$$\delta\hat{W}_f = 3\pi(1 - q_{min})\frac{r_s^2}{R^2}\left(\frac{13}{144} - \beta_{ps}^2\right). \tag{4}$$

where $\beta_{ps} = (-R/r_s^2)\int_0^{r_s} r^2(d\beta_p/dr)dr$ and β_p is the plasma poloidal normalized pressure.

Finally, the hot particle contribution (referred to with the index h) included in $\delta\hat{W}_k$ is derived from kinetic theory to include wave-particle resonances. For the modes considered in this paper and the energies expected for fast particles present in Tore-Supra experiments (about 300keV for fast ions and 50 to 80 keV for the suprathermal electrons), main wave-particle resonances are expected to take place with the particles drift precession frequency Ω_d, such that,

$$\delta\hat{W}_k = 2^{3/2}\pi^2|\mathsf{m}|\, qm_h^{3/2}\frac{\mu_0}{B_0^2} \times \int_0^a \frac{1}{r_s^2} r dr |\bar{\xi}|^2 \int_{1-r/R}^{1+r/R} d\lambda \frac{\bar{\Omega}_d^2}{\bar{\Omega}_b} \int_0^{+\infty} \mathsf{E}^{5/2} d\mathsf{E} \frac{QF_h}{\mathsf{n}\Omega_d - \omega}. \tag{5}$$

where integrations are taken over the radial and energy and anisotropy variables, $(r, \mathsf{E}, \lambda = \mu/\mathsf{E})$ (μ is the magnetic invariant). Here, QF_h is an operator acting on the hot particle distribution function F_h, such that $QF_h = \omega\partial_E F_h + \mathsf{n}\omega^{\mathsf{m}}_{*ph}/T_h$, $\bar{\xi} = \xi/(k_\theta\Psi_0/B_0\omega s)$ is the mode MHD displacement, normalized to its asymptotic values (see [17, 13]). $\bar{\Omega}_b$ and $\bar{\Omega}_d$ are the normalized particle bounce and drift frequencies (used with the convention of Ref. [2]).

A solver, MIKE (MHD Instability with Kinetic Electrons), has been developed to solve the dispersion relation (1) with the different types of inertia presented in Eqs.(2) and (3). It is based on equilibrium data derived from the CRONOS transport code and has been coupled to the C3P0/LUKE kinetic code to precisely access the complete electron distribution function in the presence of LH heating [19]. Although initially developed for fast electrons driven modes, the solver has also been used for fast ions with a more simple ion distribution function, calculated with the PION Monte-Carlo code [20] and fitted on an anisotropic Maxwellian of the form $F_h = \tilde{n}(r)\delta(\lambda - \lambda_0)e^{-\mathsf{E}/T_h(r)}$ with $\tilde{n}(r) = [n_h(r)/(2\pi m_h T_h)^{3/2}][2\bar{\Omega}_b(\lambda_0, r)]$. Explicity, $\delta\hat{W}_k$ assumed with such a distribution is

$$\begin{aligned}\delta\hat{W}_k = {} & \pi q(r_s)^2|\mathsf{m}|\int_0^a \frac{1}{r_s^2} r dr |\bar{\xi}|^2 \beta_h(r) \int_{1-r/R}^{1+r/R} d\lambda \frac{\bar{\Omega}_b(\lambda_0)\bar{\Omega}_d^2}{\bar{\Omega}_b} \times \left\{ -\frac{\mathsf{E}_{\rm res}}{T_h} Z_5(y_0) - \frac{\mathsf{E}_{\rm res}}{T_h} Z_3 \lambda \delta'(\lambda_0) \right. \\ & \left. - \frac{1}{\bar{\Omega}_d}\left[\frac{R\partial_r n_h}{n_h} Z_5(y_0) - \frac{R_0\partial_r\bar{\Omega}_b(r,\lambda_0)}{\bar{\Omega}_b(r,\lambda_0)} Z_5(y_0) + \frac{R_0\partial_r T_h}{T_h}\left(Z_7(y_0) - \frac{3}{2}Z_5(y_0)\right)\right]\right\}\end{aligned} \tag{6}$$

with $\beta_h = 2\mu_0 n_h T_h/B_0^2$, $\mathsf{E}_{\rm res} = [r/\mathsf{n}q(r)][e_h B_0 R\omega/\bar{\Omega}_d(r,\lambda_0)]$, $\sqrt{\pi}Z_p(y_0) = \int_{-\infty}^{+\infty} dy y^{p+1}\exp(-y^2)/(y^2 - y_0^2)$, for $y_0^2 = \mathsf{E}_{\rm res}/T_h$.

3.2 Beta-Alfvén Eigenmodes

In this section, the roots of the dispersion relation are compared with Tore-Supra observations, in order to determine the relevant physical ingredients determining the BAE frequency and stability.

In Ref. [5], diamagnetic effects were found to account for the BAE mode cycle during a sawtooth period at Asdex-Upgrade. Indeed, diamagnetic effects are directly related to the temperature gradient of the thermal ion population, which is known to be almost anihilated and flat in the plasma center after the sawtooth crash, and to get slowly restored during the sawtooth period. To mimic this dynamics, the dispersion relation with $\delta\hat{W}_k = \delta\hat{W}_f = 0$ is solved in Fig. 3a. for various values of the

normalized temperature gradient $\eta = (\nabla T_i/T_i)_{r_s}/(\nabla n_i/n_i)_{r_s}$ ranging from 0 to 2.0 (that is, the average gradient estimated by the TPROF code), and for several mode numbers $|n| = |m| \in [1,5]$. Although the assessed root significantly overestimates the mode experimental frequency (possibly due to a finite particle perpendicular energy [5] or to 4th order Finite Larmor Radius effects [21]), a downward shift of the order of 1 to 5 kHz is obtained in Fig. 3a. which is lower but of the same order as the experimental values in the first half of the sawtooth period (from 3 to 10 kHz). Similarly as for the experiment, a splitting occurs due the frequency $|m|$-dependence. Hence, diamagnetic effects appear as good candidates to explain the first half of the BAE cycle. Yet, from this test, they do not seem to provide a direct explanation for the second half of the sawtooth period, where the modes frequency increases significantly (up to a 30 kHz shift) while the core temperature gets stabilized.

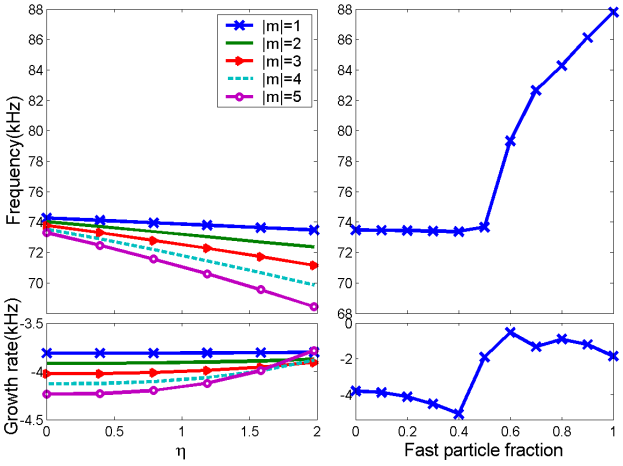

Figure 3: Evolution of the BAE frequency and growth rate with the temperature gradient, and fraction of fast particles.

Next, the non-perturbative role of the fast ion distribution is analyzed in Fig. 3c.d., using an artificial fraction ε, such that $\delta\hat{W}_k = \varepsilon\delta\hat{W}_k^{\text{experimental}}$ ($\delta\hat{W}_f$ is kept null) for the $|n| = |m| = 1$ mode (for which the use of a kink step-like MHD displacement for $\bar{\xi}$ in Eq. 5 makes some sense). As was already suggested by an earlier perturbative analysis of the BAE stability in Tore-Supra, non-perturbative effects such as a significant frequency shift (see the horizontal mismatch between theory and experiment in Fig. 12 of Ref. [2]) need to be assessed. In Fig. 3c., the frequency shift induced by the experimental distribution ($\varepsilon = 1.0$) is about 15 kHz, compared to the BAE accumulation point (given by $\varepsilon = 0$). This suggests that fast particles can have a role in the BAE frequency cycle, and that a non-perturbative treatment of stability is necessary (for such an ICRH power), in particular because such an upward shift can lead to stronger continuum damping. Nevertheless, a more refined model (for the radial structure, the role of $|n|$, details of the distribution function...) is still needed for this study (in particular, the mode excitation Fig. 3d. is too weak).

3.3 Electron fishbone modes

A similar work was carried out for the fishbone dispersion relation with the inertia (2), the fluid energy (4), and a complete electron distribution simulated by LUKE for shot #40816. In the latter shot, an oscillation was detected at a normalized radius of 0.18, which matches a reasonable q=1 surface. Its frequency was found to be relatively stable, of about 8.5kHz and interrupted by very limited frequency jumps [7], which makes it appropriate for a stability analysis. It occured for an LH power of 1MW, at a density of 2.3e-19m^{-3}.

In Fig. 4, the role of the shape of the q-profile in the fishbone stability is analyzed. For this, the q-profile is enforced in $\delta\hat{W}_k$ and chosen to be parabolic with a fixed q=1 surface at the normalized radius of 0.18, and a variable shear $s = (r/q)dq/dr$ at this point. First, this analysis is in agreement with experimental observations. Indeed the q-profile corresponding to the frequency of 8.5kHz, the growth rate is found positive. Secondly, one can note that the mode frequency and growth

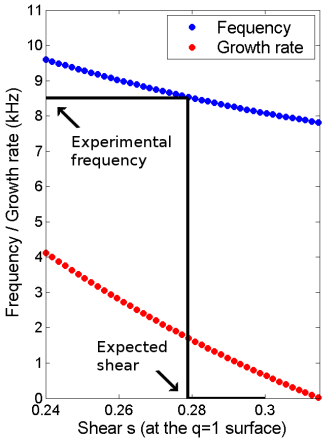

Figure 4: Evolution of the fishbone frequency and growth rate with the shear

rate are extremely sensitive to the shear. The growth rate in particular increases significantly close to its marginal point with a very small shear flattening : this is the indication that electrons characterized by a reversal of their precessional drift (whose number increases at lower shear), are fundamental for the mode excitation. This sensitivity suggests the possibility to reconstruct the q-profile from MHD observations, in particular in the presence of a cycle illustrated in Fig. 2.

4 Conditions for the existence of subcritical Beta Alfvén Eigenmodes

In this section, we study another feature of the fast particle driven stability, the existence of subcritical (linearly stable and nonlinearly unstable) modes. Finite frequency modes of the shear Alfvén spectrum which are preferentially driven by suprathermal particles, are mostly damped by resonant, Landau-like damping and continuum damping. In the nonlinear phase of a mode growth, both damping processes can be affected by the mode size or nonlinear frequency. Hence the possiblity to reach more unstable states nonlinearly.

Here, the focus is on modes which are simultaneously driven and damped resonantly. It is the case for BAEs which oscillate in a region where thermal ion Landau damping is strong, and can be resonantly driven by a population of fast ions. In order to prove the existence and triggering mechanisms of subcritical modes, a simple perturbative 1d model is used, which should be extended to non-perturbative systems as suggested in the previous section.

4.1 Model

We make use of a Poisson-Vlasov system with two species of distribution functions F_1 and F_2, whose applicability to BAEs has been discussed in Ref. [22],

$$\partial_t F_\mathrm{i} + v\partial_x F_\mathrm{i} + \frac{e_\mathrm{i}E}{m_\mathrm{i}}\partial_v F_\mathrm{i} = -\nu_\mathrm{i}\left[F_\mathrm{i} - F_{\mathrm{i}\,\mathrm{eq}}(v)\right], \quad \mathrm{i}=1,2 \tag{7}$$

$$-\partial_x E = \sum_{\mathrm{i}=1,2} e_i \int dv \left[F_\mathrm{i} - F_{\mathrm{i}\,\mathrm{eq}}(v)\right]. \tag{8}$$

excited by a initial perturbation of the form $F_1(x,v,t=0) = F_{1\mathrm{eq}}(1+\alpha\cos(kx))$. $F_{1\mathrm{eq}}$, $F_{2\mathrm{eq}}$ are the species equilibrium distribution functions given by $F_{1\,\mathrm{eq}} = [n_b/\sqrt{2\pi}v_{tb}]\exp\left(-1/2\,[v/v_{tb}]^2\right) + [n_e/\sqrt{2\pi}v_{te}]\exp\left(-1/2\,[(v-v_0)/v_{te}]^2\right)$, $F_{2\,\mathrm{eq}} = [n_d/\sqrt{2\pi}v_{td}]\exp\left(-1/2\,[v/v_{td}]^2\right)$. Hence, $F_{1\,\mathrm{eq}}$ is divided into a thermal *bulk* (index b), and a bump on tail (index e) providing resonant *excitation* and is similar to the distribution used in traditional collisional bump-on-tail models [23, 24]. F_2 has a purely thermal equilibrium distribution, intended to provide self-consistent resonant *damping* (index d).

In the perturbative limit ($n_b \gg n_e, n_d$) where the system is expected to oscillate approximately at the bulk plasma frequency, $\omega_{pb} \equiv \sqrt{n_b e_b^2/m_b}$, and assuming a cold bulk $\omega_{pb} \gg kv_b$, a slighly dissipative plasma $\omega_{pb} \gg \nu_b, \nu_e, \nu_d$ and a monochromatic perturbation, the linear bump induced resonant excitation and damping are well assessed by the independent rates γ_e and $-\gamma_d$ ($\gamma_d > 0$) (explicitely $\gamma_{s=e,d} = 0.5(\omega_{pb}/k^2)(\omega_{ps}^2/v_{ts}^2)\left|\mathrm{Im}Y\left[(\omega_{pb} - \delta_{se}kv_0)/\sqrt{2}kv_{ts}\right]\right|$, with $Y = (1+Z)$ and Z is the plasma dispersion function). When the mode amplitude is sufficiently large compared to restoring dissipative effects, $\omega_{Bs} \gg \nu_s$ (for $s = e,d$) and $\omega_{Bs} \equiv \sqrt{|e_s|Ek/m_s}$, particles get trapped inside the mode structure, leading to a reduction of the resonant contribution. In a 1-d model with Krook collision operators, the nonlinear resonant contribution has been shown to be reduced by a factor $c\nu_s^* = c\nu_s/\omega_{Bs} \ll 1$ with $\alpha = 2.0$ [23]. Following this reduction, steady-state subcritical (or *metastable*) modes can take place due to a stronger nonlinear reduction of damping compared to drive. More precisely, using modified

reduction factors of the form $\alpha\nu_s/(\alpha\nu_s+\omega_{Bs})$, we showed analytically and numerically in Ref. [25] that positive stationnary and stable solutions are possible : (i) in the complete linear region where $\gamma_L \equiv \gamma_e - \gamma_d - \nu_b > 0$, (ii) in the subcritical region, if $\gamma_{NL} \equiv \nu_e^*(\gamma_e - \nu_b) - \nu_d^*(\gamma_d + \nu_b) > 0$ and $\Delta \equiv (\gamma_{NL})^2 - 4\nu_e^*\nu_d^*\nu_b|\gamma_L| > 0$. A numerical example of the regions determined by these conditions is shown in Fig. 5 along with the different nonlinear states obtained from our Poisson model for a particular set of parameters verifying $\nu_e^*\omega_{Bb} \in [0.001, 0.1] \gg \nu_d^*\omega_{Bb} = 0.003$, and a large initial amplitude $\omega_{Bb}(0) = 0.2 > \nu_e \in [0.001, 0.1]$, $\nu_d = 0.005$. A large number of stead-state subcritical states are found corresponding to the prediction.

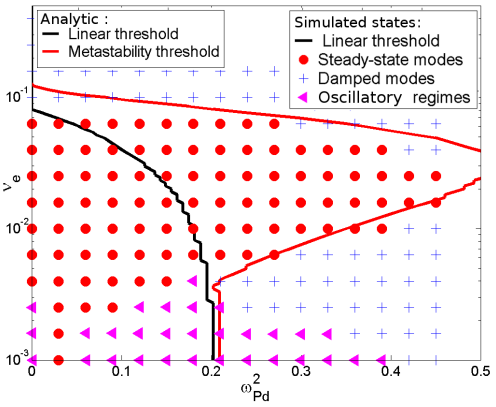

Figure 5: Simulated nonlinear states obtained, varying resonant damping and collisionality.

4.2 Refinement of the low amplitude model

The nonlinear coefficients used in the results presented in the previous paragraph, $c_s = \alpha\nu_s/(\alpha\nu_s + \omega_{Bs})$ is a fit between the quasi-linear regime ($\omega_{Bs} \to 0$) for which $c_s\gamma_s \to \gamma_s$, and the deeply trapped nonlinear regime ($\omega_{Bs} \gg \nu_s$), for which $c_s\gamma_s \to \alpha(\nu_s/\omega_{Bs})\gamma_s$. We now make use of a refined description of near-marginality ($\omega_{Bs} \to 0$), derived from the model of Ref. [26] : $c_s\gamma_s \sim \left[1 - \lambda(\omega_{Bs}/\nu_s)^4\right]\gamma_s$. Fitting this refined model with the deeply trapped regime, and assuming closeness to a saturation point ($d/dt \ll \omega_{Bs}$, $s = e, d$), the evolution of the mode amplitude follows the equation [27],

$$\frac{d\omega_{Bb}^2}{dt} = \omega_{Bb}^2\left[\frac{1+\alpha\lambda(\omega_{Be}/\nu_e)^3}{1+\alpha\lambda(\omega_{Be}/\nu_e)^3+\lambda(\omega_{Be}/\nu_e)^4}\gamma_e - \frac{1+\alpha\lambda(\omega_{Bd}/\nu_d)^3}{1+\alpha\lambda(\omega_{Bd}/\nu_d)^3+\lambda(\omega_{Bd}/\nu_d)^4}\gamma_d - \nu_b\right]. \quad (9)$$

where $\alpha = 2.0$ and $\lambda = 1/8$. Similarly as for the simple model [25] and for our set of parameters, the investigation of saturation points ($d/dt = 0$ which we solved numerically) returns one single positive stable solution in the linear unstable region, while giving zero or two solutions (a smaller unstable solution with $d/dt < 0$, and a larger stable solution with $dt > 0$) in the subcritical region. We compare the simulated amplitudes with the predicted one in Fig. 6 for all simulated steady-state modes with the fixed parameters $e_s = 1.0$ for $s = b, e, d$, $m_s = 1.0$ $s = b, e$, $n_b = 1.0, \nu_{tb} = 0.3$, $n_e = 0.03$, $\nu_{te} = 1.0$ $\nu_0 = 4.5$, $\nu_{td} = 2.5$ and $k = 0.3$, the variable parameters $(m_d/m_l, \nu_d) \in \{(2.0, 0.04), (0.5, 0.005)\}$ and full scans in $n_e \in [10^{-3}, 1]$, $\omega_{pd}^2 \in [0.0, 0.35]$.

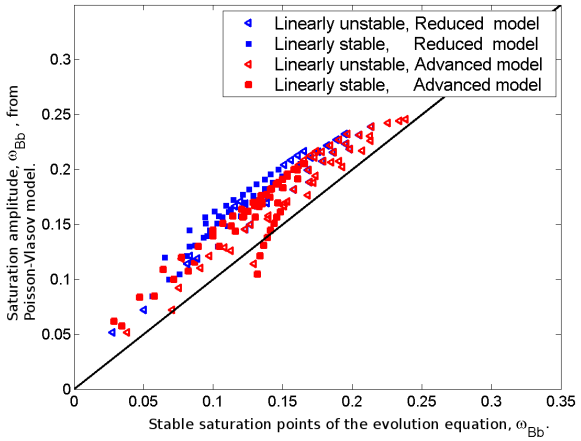

Figure 6: Comparizon between simulated and predicted saturation amplitudes.

A good agreement is found between the predicted and simulated mode amplitudes. The refined model is found to bring some improvement (17 % error, compared to 22 % for the simpler model). in particular for lower saturation amplitudes. The remaining discrepancy may be attributed to the breaking of the assumption of monochromaticity.

4.3 Triggering condition

The presented refinement is effective at low amplitudes, and in particular to assess the accuracy of the lower unstable root in the metastable region ω_{Bb}^-. From Eq. (9), a sufficient condition to obtain

a metastable mode is the use of an initial perturbation $\omega_{Bb}(0) \geq \omega_{Bb}^{-}$. It is notable that with such a model, very small perturbation amplitudes ($\omega_{Bb}^{-} \to 0$ close to marginality) can lead to much higher stable saturation amplitudes ($\propto \gamma_{\mathrm{NL}}$ close to marginality). In systems where metastability is expected, that is, when $\nu_e^* \gg \nu_d^*$, it can be easily shown that the refined model has lower roots that the simpler model, which makes the triggering of a metastable mode even easier. However, the validity if Eq. (9) is reduced to systems with a reduced time evolution, which implies an additional condition on the inertial perturbation, of the form $\omega_{Bs} > -\gamma_{\mathrm{LIN}}$ for all resonant species.

5 Conclusion

In this paper, we presented the analysis of two modes found in Tore-Supra. We put forward a particular dynamics of fast electron driven fishbones at the slow current diffusion time scale, characterized by a discontinuous frequency spectrum associated to a continuous structure evolution. Such an observation suggests an important effect of the current profile on the mode stability, which was confirmed by theory for a monotonous q-profile configuration. Next, the relevance of diamagnetic effects on Tore-Supra Beta Alfvén Eigenmodes was estimated and shown to be consistent with one part of the observed mode cycle during a sawtooth period. Indications were also given that fast particles should be considered non-perturbatively, even for non-chirping modes. Finally, we explained how subcritical Beta Alfvén Eigenmodes can take place, and presented necessary and sufficient conditions for the onset of such steady-state metastable modes. *This work was supported by the European Commission.*

References

[1] Sabot, R. et al., Nuclear Fusion **49** (2009) 085033.
[2] Nguyen, C. et al., Plasma Physics and Controlled Fusion **51** (2009) 095002.
[3] Basiuk, V. et al., Nuclear Fusion **43** (2003) 822.
[4] Guimaraes-Filho, Z.O. et al., 37 th EPS Conference on Plasma Physics (2010) P-4.125.
[5] Lauber, P. et al., Plasma Physics and Controlled Fusion **51** (2009) 124009.
[6] Cesario, R. et al., Nuclear Fusion **49** (2009) 075034.
[7] Macor, A. et al., Physical Review Letters **102** (2009) 155005.
[8] Guimaraes-Filho, Z.O. et al., 11th IAEA Conference on Energetic Particles (2009) P-10.
[9] Zonca, F. et al., 34th EPS Conference on Plasma Physics, Warsaw, Poland (2007) P-4.071.
[10] Zonca, F. et al., Plasma Physics and Controlled Fusion **38** (1996) 2011.
[11] Zonca, F. et al., Physics of Plasmas **6** (1999) 1917.
[12] Lauber, P. et al., 35 th EPS Conference on Plasma Physics (2008) 0-4.030.
[13] Nguyen, C. et al., Physics of Plasmas **15** (2008) 112502.
[14] Elfimov, A. G., Physics of Plasmas **16** (2009) 034501.
[15] Chen, L. et al., Physical Review Letters **52** (1984) 1122.
[16] White, R. B. et al., Physical Review Letters **62** (1989) 539.
[17] Zonca, F. et al., Nuclear Fusion **47** (2007) 1588.
[18] Bussac, M. N. et al., Physical Review Letters **35** (1975) 1638.
[19] Peysson, Y. et al., Joint Varenna-Lausanne International Workshop **1069** (2008) 176.
[20] Eriksson, L.-G. et al., Nuclear Fusion **33** (1993) 1037.
[21] Annibaldi, S. V. et al., Plasma Physics and Controlled Fusion **49** (2007) 475.
[22] Nguyen, C. et al., Submitted to Plasma Physics and Controlled Fusion (2010).
[23] Berk, H. L. et al., Physics of Fluids B **2** (1990) 2226.
[24] Berk, H. L. et al., Physics of Plasmas **6** (1999) 3102.
[25] Nguyen, C. et al., Submitted to Physical Review Letters (2010).
[26] Berk, H. L. et al., Physical Review Letters **76** (1996) 1256.
[27] Gorelenkov, N. N. et al., Physics of Plasmas **6** (1999) 629.